This is the accepted manuscript of the article, which has been published in *Japanese Journal of Applied Physics,* 2021, 60, SDDA06. Published 29 March 2021. https://doi.org/10.35848/1347-4065/abef0f.
This manuscript version is made available under the CC-BY-NC-ND license

Nucleation threshold of carbon black ultrasound contrast agent

Craig S. Carlson[1*], Ryunosuke Matsumoto[2], Koji Fushino[2], Miryu Shinzato[2], Nobuki Kudo[2], and Michiel Postema[1,3]

[1] *School of Electrical and Information Engineering, University of the Witwatersrand, Johannesburg, 1 Jan Smuts Laan, 2001 Braamfontein, South Africa*

[2] *Faculty of Information Science and Technology, Hokkaido University, Kita 14 Jo, Nishi 9 Chome, Kita-ku, Sapporo, Hokkaido 060-0814, Japan*

[3] *BioMediTech, Faculty of Medicine and Health Technology, Tampere University, Korkeakoulunkatu 3, 33720 Tampere, Finland*

Most ultrasound contrast agents used in ultrasonic imaging comprise shell-encapsulated microbubbles, whose ingredients have been associated with adverse bioffects. In this study, we investigated the nucleation behaviour of carbon black dispersion, whose hydrophobic nanoparticles are used intradermally. For a hypothetical, perfectly spherical carbon black particle surrounded by a perfectly spherical gaseous void, we derived a theoretical nucleation threshold of only 1.3× the resting radius. Carbon black particles and aggregates thereof were investigated using high-speed photography during 1.0-MHz sonication. The nucleation threshold found experimentally is lower than the Blake cavitation threshold of 2.0× the resting radius of free, unencapsulated microbubbles. Therefore, carbon black dispersion may be a promising ultrasound contrast agent.

Ultrasound contrast agents typically comprise lipid- or albumin-encapsulated perfluorocarbon gas microbubbles.[1–3)] They are injected during sonography with the main purposes of imaging perfusion processes and detecting tumours.[4–8)] Using acoustic transmit amplitudes sufficiently high to generate asymmetric microbubble oscillations, the presence of microbubbles is subsequently detected by means of so-called harmonic imaging.[9–11)] The encapsulating microbubbles shells and the perfluorocarbon gas ensure a prolonged lifespan of the microbubbles by several minutes to hours.[12,13)] Without an encapsulating shell, a perfluorocarbon gas microbubble would dissolve in seconds, whilst a nitrogen microbubble would dissolve in milliseconds.[14,15)]

The main disadvantage of said encapsulation materials is allergic reactions to them.[16,17)] Due to the prolonged lifespan of the microbubbles, caution should also be observed when subjecting people to sudden ambient pressure changes post contrast-agent administration, such

*E-mail: craig.carlson@wits.ac.za

as flying or scuba diving. Although the acoustic amplitudes required for harmonic imaging have been considered clinically safe, they may inadvertently generate harmonic response from surrounding tissue and associated unintended bioeffects.[18–20] Therefore, there has been an interest in ultrasound contrast agents that are safer in use than shell-encapsulated gas microbubbles and that express harmonics at lower acoustic amplitudes, *i.e.*, amplitudes that do not generate tissue harmonics.

Hydrophobic carbon black nanoparticles have demonstrated harmonic behaviour.[21] As the nucleation of carbon black nanoparticles is transient,[22] we hypothesise that harmful cavitation-related aftereffects must be less prominent when using hydrophobic carbon black instead of a microbubble-based ultrasound contrast agent. However, most carbon nanoparticles are not desirable for *in-vivo* utilisation.

Carbon black pigment dispersion is allowed to be inserted through the skin by means of needles for cosmetic reasons — the inking of a tattoo.[23] In solid state, it comprises nanoparticles or nanoparticle aggregates with a mode diameter of 0.24 μm and a maximum diameter of 0.97 μm.[24] In solution, a hydrophobic particle takes up its own volume plus a surrounding void.[25] Consequently, in solution, the carbon black pigment dispersion nanoparticles or aggregates thereof were measured to have a mode diameter of 0.29 μm and a maximum diameter of 1.14 μm.[24] In carbon black dispersion, the gaseous void surrounding the hydrophobic solid nanoparticle takes up approximately 20% of the diameter.[24] The linear resonance frequencies of these suspended nanoparticles were estimated to be greater than 15 MHz.[24] In a recent feasibility study, we found that carbon black pigment dispersion under sonication demonstrates transient nucleation.[26] In this follow-up study, we investigated the nucleation threshold of carbon black pigment dispersion nanoparticles both theoretically and experimentally.

Let us assume a perfectly spherical hydrophobic particle in suspension in an infinite liquid. Its resting radius including polytropic gaseous void is R_0, whilst its incompressible solid core radius is R_c. The instantaneous surface pressure p_s as a function of instantaneous radius R is equal to

$$p_s(R) = p_g(R) + p_v - p_L = \frac{2\sigma R}{R^2 - R_c^2}\,, \tag{1}$$

where p_L the absolute pressure in the liquid at the bubble surface, p_g is the gas pressure inside the void, p_v is the vapour pressure inside the void, and σ is the surface tension at the void–liquid interface. If there is no disturbance in the liquid pressure, *i.e.*, if the particle is at rest, $p_L = p_0$, in which p_0 is the ambient pressure, close to 1 atm.

Following the derivation of the cavitation threshold of a free bubble,[3] if buoyancy and

gas diffusion are slow with respect to a change in ambient pressure,

$$p_{\mathrm{g}}\, V^{\gamma} = \text{constant}\,, \tag{2}$$

where $V = \frac{4}{3}\pi\left(R^3 - R_{\mathrm{c}}^3\right)$ is the instantaneous void volume and γ is the ratio of specific heats of the gas. For air, $\gamma = 1.4$ is a good approximation.[3)]

Substituting (1) for the gas pressures yields

$$\left(p_0 - p_{\mathrm{v}} + \frac{2\sigma R_0}{R_0^2 - R_{\mathrm{c}}^2}\right) V_0^{\gamma} = \left(p_{\mathrm{L}} - p_{\mathrm{v}} + \frac{2\sigma R}{R^2 - R_{\mathrm{c}}^2}\right) V^{\gamma}\,, \tag{3}$$

where $V_0 = \frac{4}{3}\pi\left(R_0^3 - R_{\mathrm{c}}^3\right)$ is the resting volume of the void. Rewriting V_0 and V in terms of R and reordering gives an expression of the absolute liquid pressure as a function of instantaneous void radius:

$$p_{\mathrm{L}}(R) = \left(p_0 - p_{\mathrm{v}} + \frac{2\sigma R_0}{R_0^2 - R_{\mathrm{c}}^2}\right)\left(\frac{R_0^3 - R_{\mathrm{c}}^3}{R^3 - R_{\mathrm{c}}^3}\right)^{\gamma} + p_{\mathrm{v}} - \frac{2\sigma R}{R^2 - R_{\mathrm{c}}^2}\,. \tag{4}$$

The function $p_{\mathrm{L}}(R)$ has a minimum in point (R_θ, p_θ). If the liquid pressure is lowered below the critical threshold pressure p_θ, corresponding to threshold radius R_θ, there is no equilibrium for (4), which results in explosive expansion of R.

For microbubbles, $R_\theta \approx 2.0\, R_0$, which is referred to as the Blake cavitation threshold.[3)] A temporal pressure change $\Delta p(t) = \left[p_{\mathrm{L}}(t) - p_0\right]$ can be generated by an acoustic wave $\Delta p(t) = p_{\mathrm{a}} \sin(2\pi f t)$ of frequency f and pressure amplitude p_{a}. For the pressure change to be quasi-isostatic, f must be much less than the resonance frequencies of the suspended nanoparticles.[3)]

Using $\Delta p(t)$ as a driving function and following the derivation for an oscillating antibubble,[27)] the fundamental equation of spherical hydrophobic particle dynamics is found to be

$$R\ddot{R} + \frac{3}{2}\dot{R}^2 = \frac{1}{\rho}\left[\left(p_0 - p_{\mathrm{v}} + \frac{2\sigma R_0}{R_0^2 - R_{\mathrm{c}}^2}\right)\left(\frac{R_0^3 - R_{\mathrm{c}}^3}{R^3 - R_{\mathrm{c}}^3}\right)^{\gamma} + p_{\mathrm{v}} - \frac{2\sigma R}{R^2 - R_{\mathrm{c}}^2} - p_0 - \Delta p(t)\right]. \tag{5}$$

Assuming a low driving amplitude, the linear resonance frequency f_{r} of a spherical hydrophobic particle follows to be

$$f_{\mathrm{r}} = \frac{1}{2\pi R_0 \sqrt{\rho}} \sqrt{\frac{3\gamma\left(p_0 - p_{\mathrm{v}} + \frac{2\sigma R_0}{R_0^2 - R_{\mathrm{c}}^2}\right)}{1 - \left(\frac{R_{\mathrm{c}}}{R_0}\right)^3} - \frac{2\sigma R_0}{R_0^2 - R_{\mathrm{c}}^2}}\,, \tag{6}$$

which is similar to the linear resonance frequency of an unencapsulated antibubble.[28)] The radial dynamics of antibubbles subjected to higher acoustic amplitudes have shown to be highly nonlinear.[28)] Leaving out R_{c} from (6) gives us the linear resonance frequency of a free

gas bubble for comparison.

Solutions of (4) and (6) were computed using MATLAB® (The MathWorks, Inc., Natick, MA, USA). It was assumed that $p_0 = 1.0\,\text{atm}$, $p_\text{v} = 1.0\,\text{kPa}$, $R_\text{c} = 0.80\,R_0$, $\gamma = 1.4$, and $\sigma = 0.072\,\text{N}\,\text{m}^{-1}$. From (6) it followed that a particle of outer diameter $2R_0 \leq 1.14\,\mu\text{m}$ and core size $R_\text{c} = 0.80\,R_0$ must have a linear resonance frequency $f_\text{r} \geq 15\,\text{MHz}$. This is more than double the frequency of a free gas bubble of equal size.

The experimental procedure was identical to the experimental procedure described in Ref. 22, except for the compound under investigation and the camera frame rates.

A quantity of 0.50 μL Zuper Black pigment dispersion (INTENZE Products, Inc., Rochelle Park, NJ, USA) was pipetted into a FALCON® 15 mL High-Clarity Polypropylene Conical Tube (Corning Science México S.A. de C.V., Reynosa, Tamaulipas, Mexico), after which 5.0 mL of 049-16787 Distilled Water (FUJIFILM Wako Pure Chemical Corporation, Chuo-Ku, Osaka, Japan) was added. Tubes were either gently manually shaken for 5.0 minutes, or individually held for 1.0 minute in a 2510J-MT BRANSONIC® ULTRASONIC CLEANER (BRANSON ULTRASONICS CORPORATION, Danbury, CT, USA) filled with degassed water and operating at a transmitting frequency of 45 kHz. The sonically shaken tubes were used as controls.

From each tube, 0.2 mL was pipetted into the observation chamber of a high-speed observation system.[29] The observation chamber was placed under an Eclipse Ti inverted microscope (Nikon Corporation, Minato-ku, Tokyo, Japan) with a CFI S Plan Fluor ELWD 20XC objective lens of 20× magnification and 0.45 numerical aperture. Attached to the microscope was an HPV-X2 high-speed camera (Shimadzu, Nakagyo-ku, Kyoto, Japan), operating at frame rates equal to or greater than two million frames per second.[30] The maximum exposure time corresponded to 0.50 μs per frame. During camera recording, the material was subjected to ultrasound pulses.

A laboratory-assembled single-element transducer produced focussed ultrasound pulses.[29,30] Each pulse had a centre frequency of 1.0 MHz. It is noted that $1.0\,\text{MHz} \ll 15\,\text{MHz}$, so the pressure changes in the liquid could be considered quasi-isostatic. The voltage amplitudes of the pulses were varied from 1 V to 5 V, with 1 V increments. In a running wave field, these voltages corresponded to peak-negative acoustic pressures between 0.20 MPa and 1.0 MPa, equivalent to mechanical indices between 0.20 and 1.0.[3] To avoid a standing-wave situation, we only took the first eight ultrasonic cycles into account. The time between subsequent experiments was at least one minute. The signal fed into the transducer was generated by an AFG320 arbitrary function generator (Sony-Tektronix, Shinagawa-ku, Tokyo, Japan) and

amplified by a UOD-WB-1000 wide-band power amplifier (TOKIN Corporation, Shiroishi, Miyagi, Japan).

A total number of 87 high-speed video sequences were recorded during five imaging sessions. Each video sequence consisted of 256 frames. The video sequences were stored on a personal computer and processed offline using the `onan.m` programme in MATLAB®. In the first frame of a sequence, the rectangular area of a particle i to be sized was selected manually, after which automated adaptive thresholding was used to measure the particle cross-section areas A_{ij} per frame j.[31] The particle radii R_{ij} as a function of time t_j were computed from $R_{ij}(t_j) = \sqrt{\frac{A_{ij}}{\pi}}$. Particles oscillating out of phase with respect to the incident sound field were classified as non-nucleating, whilst particles undergoing a phase shift during sonication were classified as nucleating.

Figure 1 shows solutions of (4), expressed in Δp as a function of $R\,R_0^{-1}$. The curves had been

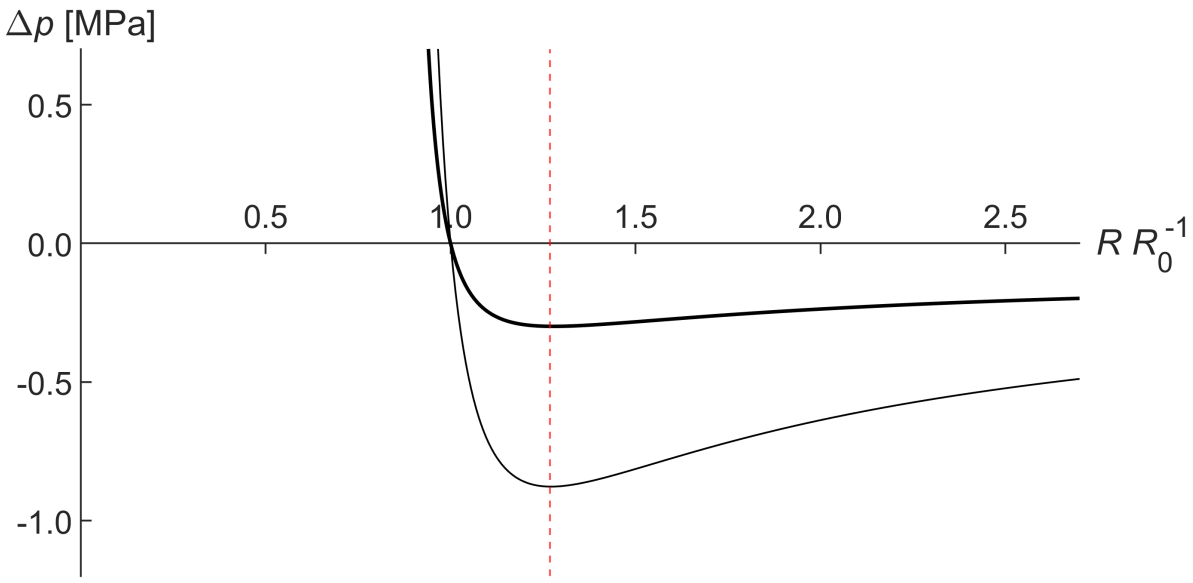

Fig. 1. Quasi-isostatic liquid pressure change Δp as a function of $\left(R\,R_0^{-1}\right)$, computed for the mode particle diameter (—) and the largest particle diameter (—) of carbon black pigment dispersion. A red dashed line is drawn through the minima, for which $R_\theta\,R_0^{-1} = 1.3$ holds (– –).

computed for the mode diameter $2R_0 = 0.29\ \mu$m with a solid core diameter $2R_c = 0.24\ \mu$m and for the largest diameter $2R_0 = 1.14\ \mu$m with a solid core diameter $2R_c = 0.97\ \mu$m. The minimum in each curve corresponds to a nucleation threshold $R_\theta\,R_0^{-1} = 1.3$. The corresponding threshold pressure change $\Delta p_\theta = p_\theta - p_0 = 0.88$ MPa for suspended nanoparticles with the mode diameter and $\Delta p_\theta = 0.30$ MPa for suspended nanoparticles with the maximum diameter.

These results indicate that carbon black pigment dispersion nanoparticles nucleate in

acoustic regimes with amplitudes less than those required for microbubble nucleation.

Figure 2 shows representative $R(t)$ curves from a high-speed video recording of Zuper Black dispersion particles. The frames were selected from the full video sequence, to illustrate

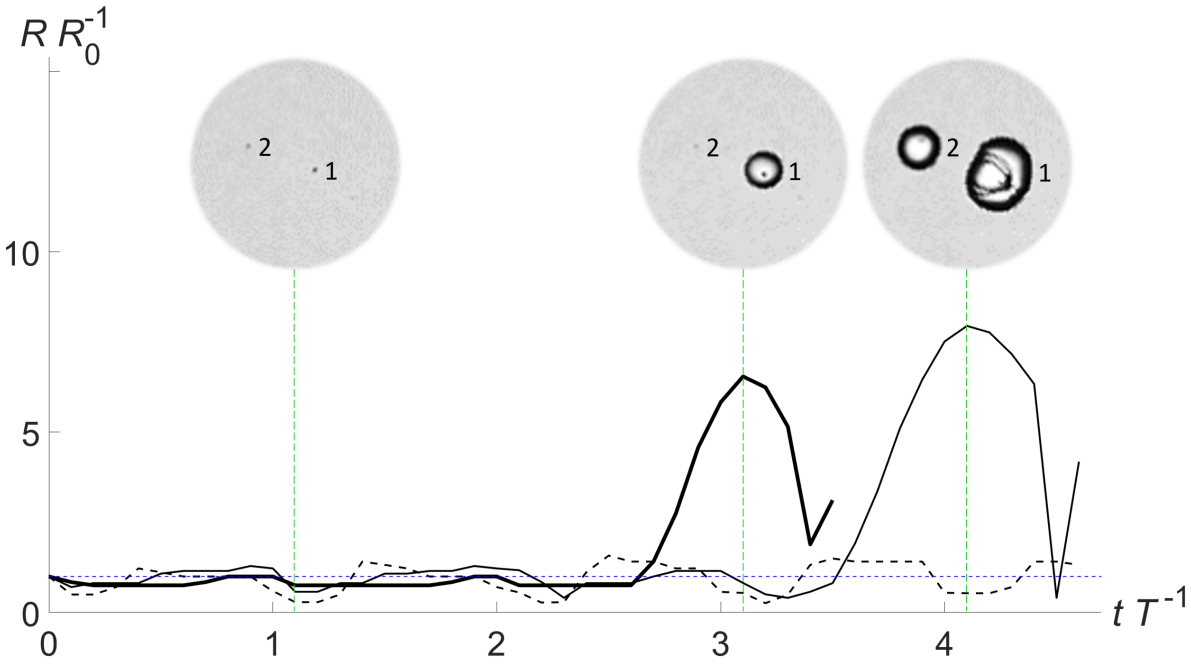

Fig. 2. Curves of the radii R of three nucleating Zuper Black dispersion particles normalised by their respective resting radii R_0 as a function of time t normalised by period T, during a 20-cycle burst with a 2-V amplitude, with 36-μm-diameter inlays of high-speed video footage. Particles 1–3 are represented by bold (—), thin (—), and dashed (– –) lines, respectively. Particle 3 is not shown in the inlays. The stationary situation $R_{max}R_0^{-1}=1$ is indicated by a blue dotted line (···).

particle sizes prior to sonication and during maximum rarefaction. Particles 1 and 2 were observed to nucleate during the third and fourth sonication cycle, respectively. Particle 1 had a maximum expansion of $R_{max}=8\times R_0$ during its first nucleation cycle, whilst particle 2 had a maximum expansion of $R_{max}=9\times R_0$ during its first nucleation sonication cycle. Particle 3, not shown in the frames but represented by the dashed $R(t)$ curve, was observed to undergo volumetric oscillations with an expansion amplitude $R_{max}=1.6\times R_0$ during sonication, $\frac{1}{2}\pi$ out of phase with respect to the incident sound field, but without explosive growth. During subsequent ultrasound pulses, the ink particles that had been involved in this nucleation cycle remained unaffected (not shown).

Figure 3 shows a histogram maximum expansion results of Zuper Black dispersion particles under sonication, normalised by their resting radii. For particles visibly undergoing

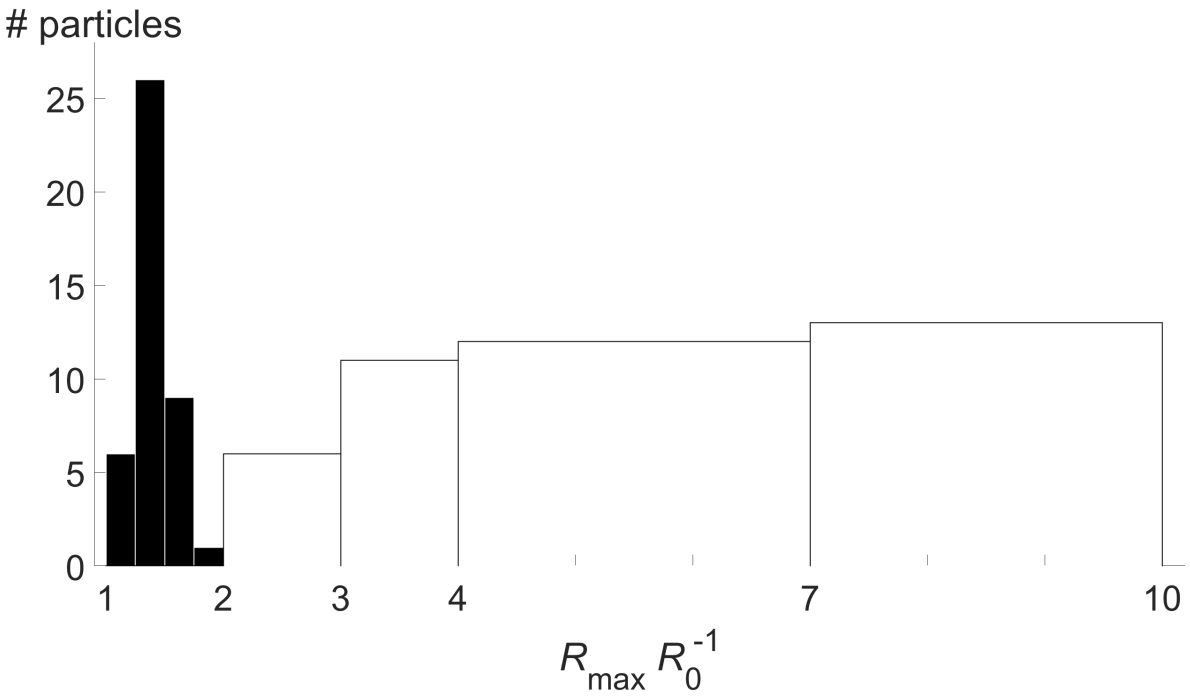

Fig. 3. Histogram of maximum Zuper Black expansion normalised by particle resting radii. White bins represent particles that underwent explosive growth, black bins represent particles that did not undergo explosive growth.

explosive growth, the maximum expansion during the first nucleation cycle was taken for $R_{\max}$, whilst for the remaining particles, the greatest expansion over all oscillation cycles was taken. All but one particle not undergoing explosive growth had a maximum expansion $R_{\max} \leq 1.75R_0$. Although the exact nucleation threshold could not be determined, these results confirm that the nucleation threshold is lower than 2× the resting radius.

Only the manually suspended ink particles demonstrated nucleation activity, whereas not a single recording of ink suspended with the ultrasonic cleaner showed nucleation. These results agree with our observations of other hydrophobic particles.[22)]

Tattoo ink particles were observed to lose part their gaseous shells. Up to five subsequent ultrasound bursts were observed to reinitiate nucleation of the same particle at the same acoustic amplitude. Sonication at a higher acoustic amplitude was also observed to renucleate particles that had stopped nucleating in a lower-amplitude regime.

It is concluded that ultrasonic nucleation of carbon black pigment dispersion nanoparticles is a transient phenomenon. The theoretical nucleation threshold of a perfectly spherical particle surrounded by a perfectly spherical gaseous void is 1.3× the resting radius of the hydrophobic nanoparticle in suspension. This is lower than the Blake cavitation threshold of

free, unencapsulated microbubbles.

Acknowledgements

This work was supported by JSPS KAKENHI, Grant Numbers JP17H00864 and JP20H04542, and by the National Research Foundation of South Africa, Grant Number 127102.

References

1) M. Chan and K. Soetanto, Jpn. J. Appl. Phys. **37**, 3078 (1998).
2) K. Soetanto and M. Chan, Ultrasound Med. Biol. **26**, 81 (2000).
3) M. Postema, *Fundamentals of Medical Ultrasonics* (Spon, London, 2011).
4) S. Tano, N. Ueno, T. Tomiyama, and K. Kimura, Clin. Radiol. **52**, 41 (1997).
5) J.-M. Correas, O. Hélénon, and J. F. Moreau, Eur. Radiol. **9**, S394 (1999).
6) H. Yoshikawa, T. Azuma, K. Sasaki, K. Kawabata, and S. Umemura, Jpn. J. Appl. Phys. **45**, 4754 (2006).
7) K. Numata, W. Luo, M. Morimoto, M. Kondo, Y. Kunishi, T. Sasaki, A. Nozaki, and K. Tanaka, World J. Radiol. **2**, 68 (2010).
8) H. Uemura, F. Sano, A. Nomiya, T. Yamamoto, M. Nakamura, Y. Miyoshi, K. Miki, K. Noguchi, S. Egawa, Y. Homma, and Y. Kubota, World J. Urol. **31**, 1123 (2013).
9) M. Kudo, *Contrast Harmonic Imaging in the Diagnosis and Treatment of Hepatic Tumors* (Springer, Tokyo, 2003).
10) K. Kawabata, N. Sugita, H. Yoshikawa, T. Azuma, and S. Umemura, Jpn. J. Appl. Phys. **44**, 4548 (2005).
11) M. Tanabe, K. Okubo, N. Tagawa, and T. Moriya, Jpn. J. Appl. Phys. **47**, 4149 (2008).
12) W. Luo, K. Numata, M. Morimoto, M. Kondo, S. Takebayashi, M. Okada, S. Morita, and K. Tanaka, Radiology **251**, 287 (2009).
13) M. Lafond, A. Watanabe, S. Yoshizawa, S. Umemura, and K. Tachibana, Sci. Rep. **8**, 7472 (2018).
14) M. Chan, K. Soetanto, and M. Okujima, Jpn. J. Appl. Phys. **35**, 3148 (1996).
15) M. Postema, A. Bouakaz, F. J. ten Cate, G. Schmitz, N. de Jong, and A. van Wamel, Ultrasonics **44**, e109 (2006).
16) C. Beavers, D. Flinchum, and M. T. Ayyoubi, Lab. Med. **44**, e129 (2013).
17) C. Hu, Y. Feng, P. Huang, and J. Jin, Medicine (Baltimore) **98**, e17745 (2019).
18) S. Umemura, K. Kawabata, and K. Sasaki, IEEE Trans. Ultrason. Ferrorelectr. Freq. Control **43**, 1054 (1996).
19) K. Tanabe, M. Belohlavek, J. F. Greenleaf, and J. B. Seward, Jpn. Circ. J. **64**, 202 (2000).
20) S. Umemura, K. Kawabata, and K. Sasaki, IEEE Trans. Ultrason. Ferrorelectr. Freq. Control **52**, 1690 (2005).
21) M. Postema, S. Phadke, A. Novell, R. Uzbekov, C. Nyamupangedengu, M. Anouti, and A. Bouakaz, Proc. 2019 IEEE AFRICON, 2019, 9133954.

22) M. Postema, R. Matsumoto, R. Shimizu, A.T. Poortinga, and N. Kudo, Jpn. J. Appl. Phys. **59**, SKKD07 (2020).
23) T. Høgsberg, K. Loeschner, D. Löf, and J. Serup, Br. J. Dermatol. **165**, 1210 (2011).
24) C. S. Carlson, A. Deroubaix, C. Penny, and M. Postema, SAIEE Afr. Res. J. **112**, 24 (2021).
25) P. Attard, Adv. Colloid Interface Sci. **104**, 75 (2003).
26) C. S. Carlson, R. Matsumoto, K. Fushino, M. Shinzato, N. Kudo, and M. Postema, Proc. 41th UltraSonic Electronics Symp., 2020, 2E5-1.
27) S. Kotopoulis, K. Johansen, O. H. Gilja, A. T. Poortinga, and M. Postema, Acta Phys. Pol. A **127**, 99 (2015).
28) N. Kudo, R. Uzbekov, R. Matsumoto, R. Shimizu, C. S. Carlson, N. Anderton, A. Deroubaix, C. Penny, A. T. Poortinga, D. M. Rubin, A. Bouakaz, and M. Postema, Jpn. J. Appl. Phys. **59**, SKKE02 (2020).
29) N. Kudo, IEEE Trans. Ultrason. Ferroelect. Freq. Control **64**, 273 (2017).
30) S. Imai and N. Kudo, Proc. IEEE Int. Ultrason. Symp., 2018, p. 184.
31) D. Bradley and G. Roth, J. Graph. Tools **12**, 13 (2007).